Journal of Operation and Automation in Power Engineering

vol. 13, no. Special Issue, Dec. 2025, Pages: 114-127

http://joape.uma.ac.ir

Research Paper

Fuel-Cost Reduction and Energy-Efficient Control of Plug-in Hybrid Electric Vehicles Using Fuzzy Cognitive Maps by Optimization of Control Strategy in Real Traffic Conditions

Anber Abraheem Shlash Mohammad [1,*], *Suleiman Ibrahim Mohammad* [2], *Asokan Vasudevan* [3], *Javohir Zokirov* [4], *Gulchexra Khlmatjanova* [5], *Nodirakhan Jurayeva* [6], *Alisher Yunusov* [5], *Zakir Tadjibaev* [6], *Muazzamkhon Mannopova* [7], and *Abdullaeva Shakhnoza* [7]

[1]*Digital Marketing Department, Faculty of Administrative and Financial Sciences, University of Petra, Jordan.*
[2]*Department of Business Administration, Business School, Al Al-Bayt University, Mafraq 25113, Jordan.*
[3]*Faculty of Business and Communications, INTI International University, 71800 Negeri Sembilan, Malaysia.*
[4]*Termiz University of Economics and Service, Farovon Street 4-b, Termez, Surxondaryo, Uzbekistan.*
[5]*Candidate of Economic Sciences, Fergana State University, Murabbiylar Street, Home 19, Fergana, Uzbekistan.*
[6]*Department of World and Regional Economics, Fergana State University, Murabbiylar Street, Home 19, Fergana, Uzbekistan.*
[7]*Fergana State University, Murabbiylar Street, Home 19, Fergana, Uzbekistan.*

Abstract— *This study introduces a novel supervisory control framework based on Fuzzy Cognitive Maps (FCM) for optimal energy management in plug-in hybrid electric vehicles (PHEVs). The proposed supervisory controller is structured to simultaneously satisfy the driver's demanded power, maintain the battery state of charge (SOC) within an acceptable operating range, and reduce fuel consumption. Owing to the fact that the presented method does not require an accurate system model, the computational burden associated with deriving the control policy is significantly reduced, and the overall implementation becomes less complex compared with classical control approaches. The target PHEV considered in this research features a series–parallel powertrain architecture. To evaluate the effectiveness of the proposed control strategy, simulations are conducted using three standard driving cycles along with an urban driving cycle representative of metropolitans. The results demonstrate that the proposed FCM-based supervisory controller not only fulfills the demanded traction power but also lowers fuel consumption relative to conventional fuzzy controllers, while maintaining the SOC within an appropriate operational window.*

Keywords—Plug-in hybrid electric vehicle, fuzzy cognitive maps, supervisory control, energy management, state of charge.

1. INTRODUCTION

The rapidly increasing global demand for sustainable transportation, growing concerns regarding greenhouse gas emissions, and fluctuations in fossil fuel prices have accelerated the shift toward electrified mobility [1]. Among the various electrified transportation technologies, PHEVs have emerged as a practical and scalable solution due to their ability to combine the high efficiency of electric propulsion with the extended driving range of Internal Combustion Engines (ICEs) [2]. By enabling external charging and dual-source energy utilization, PHEVs offer significant potential in reducing fuel consumption, increasing energy efficiency, and lowering environmental impact [3]. Consequently, the design of intelligent and robust energy management strategies (EMSs) has become a central focus of contemporary research efforts in automotive control and powertrain optimization [4].

A key challenge in PHEV powertrain operation is the development of an EMS capable of coordinating energy flow between the engine, electric motor, and battery to minimize fuel consumption while maintaining the battery SOC within safe limits and simultaneously satisfying driver power demand [5]. Achieving these objectives is non-trivial due to the nonlinear, multi-domain, and time-varying nature of PHEV dynamics. Uncertainties associated with driving behavior, traffic conditions, system degradation, and environmental factors further complicate real-time control [6]. As a result, designing EMSs that ensure high performance, robustness, and computational efficiency has remained an open research problem, attracting substantial attention in recent years [7].

Historically, a wide spectrum of EMS approaches has been introduced. Rule-based strategies, including deterministic rules and

Received: 30 Nov. 2025
Revised: 23 Dec. 2025
Accepted: 25 Dec. 2025
*Corresponding author:
E-mail: mohammad197119@yahoo.com (A.A. Shlash Mohammad)
DOI: 10.22098/joape.2025.18936.2475

fuzzy-logic-based controllers, have been widely employed because of their simplicity, ease of implementation, and robustness to modeling uncertainties [8]. However, classical fuzzy controllers rely heavily on expert knowledge, have limited adaptability, and may not provide globally optimal behaviors, particularly under rapidly varying driving conditions [9]. Optimization-based EMS techniques—including Dynamic Programming (DP), Model Predictive Control (MPC), and Pontryagin's Minimum Principle (PMP)—have demonstrated strong theoretical performance in fuel-saving applications [10]. However, their practical use in onboard controllers remains limited [11]. DP suffers from prohibitive computational burden and requires complete knowledge of the driving cycle [12]; MPC depends heavily on accurate prediction models and involves solving constrained optimization problems online; and PMP, while computationally lighter, is sensitive to variations in driving patterns and typically requires heuristic adjustment of co-states [13]. More recently, learning-based strategies such as Reinforcement Learning (RL) and deep RL have been proposed to improve adaptability under uncertain environments [14]. Despite promising results, these methods often require extensive training datasets, may exhibit stability issues, and impose substantial computational costs that challenge real-time implementation in production vehicles [15]. These limitations have motivated the exploration of alternative supervisory control approaches that retain the interpretability and low computational complexity of rule-based systems while offering enhanced adaptability. Fuzzy Cognitive Maps (FCMs) provide such a framework: they capture causal relationships among key powertrain variables, require minimal reliance on detailed mathematical models, and support adaptive tuning mechanisms with significantly lower computational overhead compared to optimization-based or learning-based EMS schemes.

More recently, learning-based approaches, particularly RL and deep reinforcement learning (DRL), have been extensively investigated for EMS design. DRL frameworks based on deep Q-networks and actor–critic structures have been applied to hybrid and plug-in hybrid vehicles, showing improved fuel economy and adaptability compared with fixed rule-based strategies [16]. Multi-objective DRL formulations have also been proposed to jointly optimize fuel consumption, driving comfort, and battery degradation, thereby embedding battery health considerations directly into the reward function [17]. In parallel, adaptive DRL-based ECMS schemes correct equivalent factors online using DDQN or similar algorithms informed by SOC and predicted driving-cycle information, enhancing robustness under varying traffic conditions [18]. Although these RL-based EMSs achieve promising performance, they typically require extensive offline training data, careful hyperparameter tuning, and non-trivial onboard computational resources, which can complicate real-time implementation in production ECUs. In light of these limitations, there is growing interest in alternative intelligent supervisory control frameworks that can combine the advantages of rule-based systems and learning-oriented structures while maintaining low computational complexity and reducing dependency on accurate mathematical models [19]. One promising candidate in this direction is the family of FCMs. Originally introduced as a knowledge-based modeling framework, FCMs represent causal relationships among system variables using fuzzy weighted connections, allowing concept-level reasoning and inference with low computational overhead [20]. Owing to their transparency, interpretability, and ability to encode expert knowledge while supporting adaptive mechanisms, FCMs have recently gained attention in several control and decision-making applications [21].

Consequently, FCMs offer a compelling balance between interpretability, adaptability, and computational efficiency—properties that are especially desirable for real-time supervisory control of complex hybrid powertrains. The application of FCMs to EMS design for hybrid vehicles is still relatively limited but is expanding. FCM-based supervisory control offers multiple advantages:

1) It eliminates the need for an accurate model of the nonlinear PHEV powertrain,
2) It supports rapid online inference with low computational cost,
3) It can integrate expert knowledge in a structured manner, and
4) It provides flexibility to incorporate learning schemes or rule-adjustment mechanisms.

A recent study demonstrated that an FCM-based controller can successfully regulate SOC and reduce fuel consumption in comparison with classical fuzzy controllers under a variety of driving conditions [22]. However, existing works remain relatively scarce, and several important aspects have not yet been fully addressed. Most FCM-based EMS implementations focus on comparatively simple hybrid powertrain topologies and rely on heuristic or single-objective tuning of the FCM weights, often evaluated exclusively on standard driving cycles [23]. In particular, the potential of FCMs for real-world supervisory control in complex series–parallel PHEV architectures, their systematic integration into hierarchical controller structures with local actuators, and their multi-objective calibration for simultaneous SOC regulation and fuel economy optimization have not been comprehensively investigated [24].

Moreover, many previous EMS studies [24, 25] have been limited by over-reliance on standard driving cycles such as NEDC, WLTC, or UDDS, which do not fully represent real-world traffic patterns, frequent stop-and-go scenarios, or congested urban environments. To ensure practical applicability, it is essential to evaluate control strategies using both standardized test cycles and region-specific real driving conditions [26]. The lack of such comprehensive validation emphasizes a critical gap in the current literature.

Motivated by these observations, the present study develops and evaluates a novel FCM-based supervisory control structure for energy management in a plug-in hybrid electric vehicle equipped with a series–parallel powertrain architecture. In contrast to [22] and other existing FCM-based schemes, the proposed approach: (i) explicitly targets a complex series–parallel topology with multiple operating modes; (ii) employs a two-stage FCM design, in which an initial qualitative map capturing dominant causal relationships is extended into a supervisory FCM that generates reference signals for three local PI controllers (engine, motor, and generator); and (iii) tunes both the initial and supervisory FCM parameters using an Estimation of Distribution Algorithm (EDA) driven by a multi-objective cost function that jointly penalizes SOC deviation and fuel consumption. Furthermore, the controller is evaluated under both standard driving cycles and a real-world metropolitan's urban cycle, providing a more comprehensive assessment of its practical performance than studies restricted to idealized driving profiles. Although the proposed controller indirectly reduces pollutant emissions through lower fuel consumption, explicit emissions modeling is beyond the scope of the present study. Accordingly, the title and related statements have been amended for clarity.

Unlike optimization-based approaches, the proposed strategy does not require a detailed system model or computationally intensive online calculations. In contrast to classical fuzzy controllers, the FCM structure incorporates causal knowledge among key variables, enabling more coherent reasoning and superior adaptability. Furthermore, the causal mapping mechanism makes the controller adaptable to different driving conditions without structural changes. To assess the effectiveness and robustness of the proposed method, simulations are conducted across three widely used standard driving cycles as well as a representative real-world urban driving cycle from metropolitan, characterized by dense traffic and frequent stop-and-go behavior. This comprehensive testing scenario enables a more realistic evaluation of the controller's practical performance. Simulation results indicate that the proposed FCM-based supervisory strategy achieves lower fuel consumption compared with conventional fuzzy rule-based controllers while maintaining SOC stability and

fully satisfying driver power demand. Overall, the contributions of this work are threefold:

1) The development of a hierarchical supervisory EMS based on a two-stage FCM structure specifically tailored to series–parallel PHEVs and interfaced with dedicated local PI controllers for the ICE, electric motor, and generator;
2) The formulation and implementation of an EDA-based multi-objective identification procedure for the FCM parameters, in which SOC regulation and fuel consumption are jointly optimized; and
3) The comprehensive validation of the proposed FCM-based strategy against a conventional fuzzy rule-based EMS under both standard (UDDS, NEDC, WLTC) and real-world (metropolitans urban) driving cycles, demonstrating improvements in fuel consumption, SOC stability, generator torque smoothness, and computational efficiency.

2. Vehicle Modeling

In the design of hybrid and plug-in hybrid electric vehicles (HEVs and PHEVs), four primary powertrain architectures are commonly employed: series, parallel, series–parallel, and complex (power-split) configurations. Each structure offers distinct operational characteristics and trade-offs in terms of efficiency, controllability, and component utilization. The vehicle considered in this study adopts a series–parallel powertrain, which integrates the advantages of both series and parallel configurations to enhance operational flexibility, energy efficiency, and fuel economy.

The series–parallel configuration was selected because it reflects the architecture used in a wide range of contemporary commercial PHEVs (e.g., Toyota Prius Plug-In, Hyundai Ioniq PHEV, Ford Fusion Energi). This topology offers high operational flexibility by allowing propulsion from the electric motor, the ICE, or both, while also supporting engine-driven battery charging. Such flexibility makes the series–parallel layout an appropriate platform for evaluating supervisory control strategies, as it includes all major operating modes relevant to real-world hybrid operation. Moreover, compared with purely series or purely parallel structures, the series–parallel configuration provides a richer interaction between components, enabling a more meaningful assessment of the proposed FCM-based coordination method. The main subsystems of a plug-in hybrid electric vehicle include the electric traction motor, generator, ICE, high-voltage battery pack, and the vehicle dynamics module. These components interact through mechanical and electrical couplings to provide traction power, regulate energy flow, and ensure stable operation across different driving conditions. A simplified schematic of the interconnections among the powertrain components—illustrating the flow paths between the engine, generator, electric motor, and battery—is presented in Fig. 1.

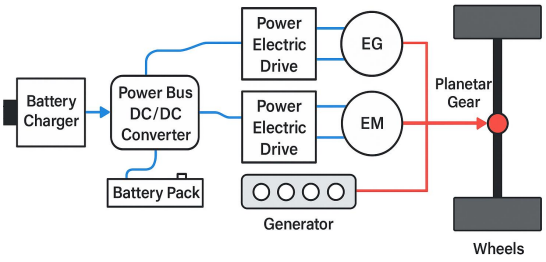

Fig. 1. Modern schematic representation of the series–parallel plug-in hybrid electric vehicle (PHEV) powertrain architecture.

2.1. Longitudinal vehicle dynamics

The longitudinal motion of the vehicle is governed by Newton's second law:

$$m \cdot \dot{v}(t) = F_{\text{trac}}(t) - F_{\text{res}}(t) \tag{1}$$

where m is the total vehicle mass, $v\cdot(t)$ is the longitudinal acceleration, F_{trac} is the traction force generated at the wheels, F_{res} is the total resistive force.

The resistive force is composed of aerodynamic drag, rolling resistance, and road grade resistance:

$$F_{\text{res}} = F_{\text{aero}} + F_{\text{roll}} + F_{\text{grade}} \tag{2}$$

The aerodynamic drag is modeled as:

$$F_{\text{aero}} = \frac{1}{2}\rho A_f C_d v^2 \tag{3}$$

Rolling resistance is given by:

$$F_{\text{roll}} = mgC_r \cos(\theta) \tag{4}$$

The grade (slope) resistance is expressed as:

$$F_{\text{grade}} = mg \sin(\theta) \tag{5}$$

The traction force at the wheels relates to the motor/engine torque via the transmission ratio:

$$F_{\text{trac}} = \frac{T_{\text{wh}}}{R} \tag{6}$$

where R is the wheel radius.

2.2. ICE model

The ICE behavior is represented using a static fuel consumption map that relates engine torque and speed to fuel flow rate:

$$\dot{m}_f = f\left(\omega_{\text{ICE}},\ T_{\text{ICE}}\right) \tag{7}$$

Engine output power is:

$$P_{\text{ICE}} = T_{\text{ICE}} \cdot \omega_{\text{ICE}} \tag{8}$$

The engine is coupled to the generator through a clutch, enabling its operation in efficient regions of its BSFC map.

2.3. Electric motor and generator models

The electric traction motor provides propulsion torque according to:

$$T_m = k_t i_q \tag{9}$$

The motor electrical power is:

$$P_m = T_m \cdot \omega_m \tag{10}$$

Similarly, the generator produces electrical power:

$$P_g = \eta_g T_g \cdot \omega_g \tag{11}$$

where η_g is the generator efficiency.

Motor and generator losses are captured using efficiency maps stored as lookup tables.

2.4. Battery model and SOC dynamics

The battery is modeled using an equivalent-circuit representation with open-circuit voltage and ohmic resistance:

$$V_b = E_{\mathrm{OCV}}(SOC) - i_b R_b \tag{12}$$

Battery power is:

$$P_b = V_b \cdot i_b \tag{13}$$

The State of Charge (SOC) dynamic equation is:

$$\dot{SOC} = -\frac{\eta_b P_b}{V_{\mathrm{nom}} Q_{\mathrm{cap}}} \tag{14}$$

where η_b is charging/discharging efficiency, V_{nom} is nominal battery voltage, Q_{cap} is battery capacity.

2.5. Powertrain operating modes

The series–parallel architecture supports the following operational modes:

A) Electric drive mode

$$P_{\mathrm{req}} = P_m \tag{15}$$

B) Engine drive mode

$$P_{\mathrm{req}} = P_{\mathrm{ICE}} \tag{16}$$

C) Hybrid traction mode

$$P_{\mathrm{req}} = P_{\mathrm{ICE}} + P_m \tag{17}$$

D) Charging mode (Engine–Generator)

$$P_b = P_g - P_m \tag{18}$$

E) Regenerative braking mode

$$P_b = \eta_r P_{\mathrm{regen}} \tag{19}$$

This mode classification is essential for the supervisory controller based on Fuzzy Cognitive Maps (FCM) developed in the following section.

The PHEV considered in this study has been modeled using the ADVISOR simulation platform, which allows for detailed representation of powertrain components and vehicle-level behavior. The technical specifications of the selected vehicle are summarized in Table 1. These parameters include the main geometric and dynamic characteristics, ICE ratings, electric motor and generator capabilities, and the battery system properties that collectively define the vehicle's operational envelope. The ADVISOR configuration employed in this study is based on a validated mid-size PHEV template included in the ADVISOR library. Component parameters such as battery capacity, nominal voltage, motor power rating, generator efficiency, and engine displacement were drawn directly from ADVISOR's benchmark datasets and supplemented with values representative of modern production PHEVs reported in manufacturer technical specifications and prior studies [3, 22]. This ensures that the simulated powertrain behavior lies within realistic operational ranges and reflects the performance characteristics of commercially available vehicles. The engine's Brake Specific Fuel Consumption (BSFC) map and the efficiency maps of the electric motor and generator are likewise taken from experimentally validated datasets distributed with ADVISOR, which have been widely used in energy-management research. Therefore, the simulation platform rests on component-level models that are well established and extensively benchmarked.

Table 1. Vehicle specifications used in this study.

Section	Parameter	Value
Vehicle	Mass (kg)	1750
	Frontal surface area (m^2)	2.3
	Wheelbase (m)	1.3
	CG distance from front axle (m)	1.35
	CG distance from rear axle (m)	1.55
ICE	Rated power (kW)	110
	Rated speed (rpm)	5000
	Maximum speed (rpm)	6000
Electric Motor	Rated power (kW)	50
Generator	Rated power (kW)	120
Battery	Nominal voltage (V)	270
	Capacity (Ah)	71
	Number of cells (series)	10
	Number of parallel sets	10

To assess the robustness of the simulation environment, a sensitivity check was performed on several influential parameters, including battery capacity (±10%), motor and generator efficiencies (±5%), and engine fuel-consumption map scaling (±5%). These variations produced expected quantitative changes in total fuel consumption but did not alter the qualitative trends or the relative performance advantage of the proposed FCM-based controller compared with the fuzzy baseline. This indicates that the conclusions of the study are not overly sensitive to the precise numerical values of individual components and that the supervisory behavior of the FCM controller generalizes well within realistic parameter variation ranges. The dynamic model of the plug-in hybrid electric vehicle exhibits a high degree of complexity due to the simultaneous interaction between mechanical and electrical subsystems. As a result, a simplified yet sufficiently accurate representation is required to ensure reliable simulation without imposing excessive computational cost. The ADVISOR environment provides an appropriate balance by incorporating experimentally validated component models, enabling system-level analysis while preserving essential nonlinear behaviors.

It should be noted that the accuracy of the energy management strategy directly depends on the fidelity of the underlying component models. The hybrid powertrain includes multiple coupled subsystems—engine, generator, electric motor, battery, and transmission—each contributing to the overall dynamics. Therefore, the model configuration must capture transient responses, steady-state characteristics, and efficiency maps to support realistic evaluation of the supervisory control strategy.

By integrating these component descriptions into a unified simulation framework, the model employed in this study offers a reliable platform for assessing the performance of the proposed FCM-based supervisory controller under standard and real-world driving cycles. This modeling approach ensures that the predicted behavior of the vehicle remains consistent with physical constraints and operational principles observed in practical PHEV architectures. All symbols used in Section 2 are listed in Table 2 along with their values and sources.

3. Fuzzy Cognitive Maps

The concept of cognitive maps was first introduced by Axelrod as a qualitative tool for representing and analyzing decision-making processes in complex social systems. Building on this idea, later extended the framework and proposed Fuzzy Cognitive Maps

Table 2. Complete parameter set used in the vehicle and component models.

Parameter	Symbol	Value	Unit	Source
Vehicle mass	m	1750	kg	ADVISOR default / Manufacturer spec
Frontal area	A_f	2.3	m^2	ADVISOR
Drag coefficient	C_d	0.32	–	Literature / ADVISOR
Rolling resistance coefficient	C_{rr}	0.015	–	ADVISOR
Wheel radius	R	0.31	m	ADVISOR
Air density	ρ	1.225	kg/m^3	ISO standard
Engine rated power	–	110	kW	Manufacturer database
Engine rated speed	–	5000	rpm	Manufacturer database
Engine max speed	–	6000	rpm	Manufacturer database
EM rated power	–	50	kW	ADVISOR
Generator rated power	–	120	kW	ADVISOR
Generator efficiency	η	0.92	–	ADVISOR map
Battery nominal voltage	V_{nom}	270	V	ADVISOR
Battery capacity	Q_{cap}	71	Ah	ADVISOR
Number of cells (series)	–	10	–	ADVISOR
Number of parallel sets	–	10	–	ADVISOR
Battery resistance	R_b	0.035	Ω	ADVISOR
Battery efficiency	η_b	0.96	–	Literature
Gravitational acceleration	g	9.81	m/s^2	–
Activation function steepness (FCM)	λ	1.0	–	Identified via EDA
Learning rate (EDA)	η	0.05	–	Selected experimentally
FCM update frequency	–	1	Hz	Control architecture
PI controller frequency	–	10	Hz	Control architecture

(FCMs) as a powerful method for modeling the dynamic behavior of complex systems using fuzzy logic and graph theory. In an FCM, system behavior is captured through a set of interacting "concepts" and the causal relationships among them, enabling a compact and interpretable representation of qualitative knowledge and dynamic interactions.

An FCM can be formally described as a directed graph composed of N nodes (concepts) and weighted edges. Each node C_iCi represents a concept, state, or variable of the system (e.g., driver power demand, battery SOC, fuel consumption), and each directed edge from concept C_j to concept C_i is associated with a fuzzy weight w_{ij}. The weight w_{ij} encodes both the strength and polarity of the causal influence of C_i on C_j : positive values indicate an excitatory effect, negative values indicate an inhibitory effect, and values close to zero represent weak or negligible causal influence. The entire structure can be represented in matrix form by an $N \times N$ adjacency (weight) matrix $W = [w_{ij}]$.

The state of each concept at iteration k is denoted by $C_i(k)$, typically normalized to lie within a bounded interval, such as [0,1] or [-1,1]. The dynamic evolution of the FCM is governed by an iterative update rule in which the new value of each concept is computed as a nonlinear function of the weighted sum of the values of the concepts that influence it. A common formulation of the FCM state-update equation is:

$$C_i(k+1) = f\left(C_i(k) + \sum_{j=1}^{N} w_{ij} C_j(k)\right), \quad i = 1, 2, \ldots, N \tag{20}$$

where $C_i(k)$ is the value of concept i at iteration k, w_{ij} denotes the causal weight from concept j to concept i, and $f(\cdot)$ is a bounded activation (threshold) function. Typical choices for $f(\cdot)$ include the sigmoidal, hyperbolic tangent, or saturated linear functions, for example:

$$f(x) = \frac{1}{1 + e^{-\lambda x}} \tag{21}$$

where $\lambda > 0$ controls the steepness of the transition. Through repeated application of the update rule, the concept values may converge to a fixed point, enter a limit cycle, or exhibit more complex dynamic patterns, thereby reflecting the qualitative behavior of the underlying system.

In the present work, each concept $C_i(k)$ is defined as a normalized, dimensionless representation of an underlying physical variable $x_i(k)$ (e.g., SOC, vehicle speed, engine speed, torque demand). Physical variables are mapped to the interval [0, 1] using a min–max scaling:

$$C_i\,(k) = \text{sat}_{[0,1]}\left(\frac{x_i(k) - x_i^{\min}}{x_i^{\max} - x_i^{\min}}\right) \tag{22}$$

where ${x_i}^{minx}$ and ${x_i}^{max}$ denote the lower and upper bounds for variable x_i, and sat[0,1](·) denotes saturation (clipping) to the [0,1] interval. This scaling ensures that all concepts share a common numerical range while preserving the relative magnitude and ordering of the underlying physical quantities.

An important feature of FCMs is their ability to learn, refine, and extend the causal structure over time. In practical applications, it is often unrealistic or impossible to specify all causal relationships and weights exactly at the design stage due to system complexity and the large number of interacting variables. Instead, an initial map is constructed using partial expert knowledge, and the weights are subsequently adjusted using data-driven learning rules. A widely used adaptation mechanism is based on a Hebbian-type

learning law, which can be expressed as:

$$\Delta w_{ij}(k) = \eta C_i(k) C_j(k) \tag{23a}$$

or, in a normalized (orregularized) form,

$$w_{ij}(k+1) = \tag{23b}$$

$$w_{ij}(k) + \eta \left[C_i(k) C_j(k) - \lambda w_{ij}(k) \right]$$

where $\eta > 0$ is the learning rate and $\lambda \geq 0$ is a forgetting factor. These rules enable incremental tuning of the causal weights based on observed concept activations, allowing the FCM to better capture the actual dynamics of the system as new data become available.

Because of this capability for incremental refinement, it is not necessary for the initial FCM to fully encode all causal links or precise numerical weights. In many real-world applications involving complex and nonlinear dynamical systems, the exact structure and parameters are partially unknown or only qualitatively understood. The FCM framework allows the designer to start from a coarse, high-level cognitive model containing only the most relevant concepts and dominant causal relationships and then systematically expand or adjust the map. The impact of newly added concepts and updated weights on the overall system behavior can be analyzed through simulation and sensitivity analysis. In summary, FCMs provide an effective modeling paradigm for complex dynamical systems in which both qualitative expert knowledge and quantitative data must be combined. By representing the system as a network of interacting concepts with fuzzy causal links, FCMs offer interpretability, low computational complexity, and an inherent capacity for learning and adaptation, making them particularly suitable as supervisory decision-making tools in applications such as energy management of plug-in hybrid electric vehicles.

4. FCM-Based Supervisory Control

A PHEV is an inherently complex dynamical system with strong couplings between mechanical and electrical subsystems, nonlinear component characteristics, and multiple operating modes. This structural complexity makes the direct design of a single centralized controller using classical or modern control techniques difficult and often impractical. A more suitable approach for such systems is to decompose the overall powertrain into several interacting subsystems, design a local controller for each subsystem, and then coordinate these local controllers through a higher-level supervisory controller. It should be emphasized that, unlike previous FCM-based EMS implementations in the literature, the extended supervisory FCM in this work is explicitly embedded into a hierarchical control architecture, where it generates reference signals for local PI controllers based on a multi-objective EDA-tuned causal structure, thereby enabling systematic coordination of the ICE, EM, and EG in a series–parallel PHEV powertrain.

Table 3 summarizes the relative characteristics of major EMS categories considered in the literature. As shown, the proposed FCM-based supervisor occupies an advantageous middle ground between purely rule-based and learning-based strategies. It preserves interpretability and low computational cost while introducing adaptability and causal reasoning that traditional fuzzy systems lack. This comparison highlights the motivation for adopting FCMs in supervisory energy management.

From an energy-management perspective, the considered PHEV can be partitioned into three main subsystems:

1) **Electric traction motor (EM):** Responsible for providing a portion of the traction torque demanded at the wheels.
2) **ICE:** Responsible both for supplying part of the traction power and for driving the electrical generator.
3) **Electrical generator (EG):** Responsible primarily for recharging the battery during vehicle operation.

In the proposed control structure, a dedicated local PI controller is assigned to each of these subsystems. The electric motor controller (CEM) regulates the motor torque, the generator controller (CEG) regulates the generator torque, and the engine controller (CICE) regulates the engine speed and torque. A supervisory controller based on FCM provides the reference signals for these three local controllers, thereby coordinating their actions to satisfy driver demand, maintain the battery state of charge (SOC) within a prescribed range, and reduce fuel consumption.

A schematic block diagram of the proposed control strategy is depicted conceptually in Fig. 2. At each sampling instant, the actual vehicle speed is compared with the driver's demanded speed, and a reference longitudinal acceleration is computed by a conventional speed-control loop. The following quantities are then supplied as inputs to the FCM-based supervisory controller:

- current vehicle speed,
- reference acceleration,
- battery state of charge (SOC),
- ICE speed in revolutions per minute (RPM_{ICE}).

Based on these inputs, the FCM-based supervisor determines the reference values required by the three local controllers, namely:

- reference electric motor speed ${RPM_{EM}}^{Ref}$,
- reference engine speed ${RPM_{ICE}}^{Ref}$,
- reference generator torque for battery charging ${T_{Batt}}^{Ref}$,
- reference acceleration command $\mathrm{Acc_{Ref}}$ produced by the speed controller.

The PI controllers C_{EM}, C_{EG}, and C_{IC} then track these references to generate appropriate torque commands for the EM, EG, and ICE, respectively.

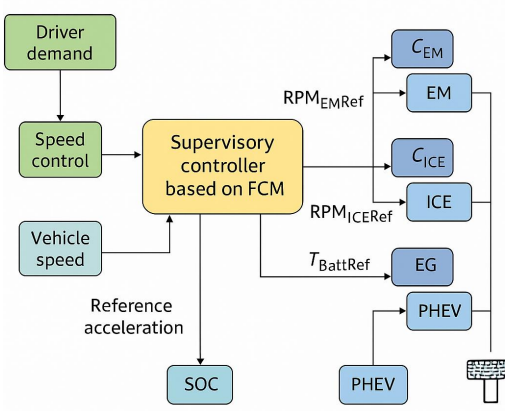

Fig. 2. Block diagram of the proposed supervisory control strategy based on Fuzzy Cognitive Maps (FCM).

4.1. Initial FCM structure

The supervisory controller is constructed in two main stages. In the first stage, an initial FCM is defined based on available qualitative knowledge of the PHEV powertrain. The concepts included in this initial map are:

- battery state of charge: SOC,
- electric motor speed: RPM_{EM},
- generator speed: RPM_{EG},
- engine speed: RPM_{ICE},
- engine torque: TI_{CE},
- requested torque from the electric motor: ${T_{EM}}^{Req}$,
- requested torque from the generator: ${T_{EG}}^{Req}$,
- demanded throttle opening: Thr,
- vehicle speed variation: ΔV,
- fuel consumption: Fuel.

These eleven concepts and their twelve causal relationships form the initial FCM used to model the qualitative dynamic behavior of

Table 3. Comparison of major EMS approaches for PHEVs.

Criterion / Feature	**Classical fuzzy EMS**	**Optimization-based EMS (DP, MPC, PMP)**	**RL-based EMS**	**Proposed FCM-based supervisor**
Model dependency	Low (expert rules; no explicit model required)	High (requires accurate dynamic & predictive models)	Medium–High (model-free RL needs large training data; model-based RL requires approximate models)	Low–Medium (qualitative causal structure + data-driven weight tuning)
Computational burden	Very low	High (DP offline, MPC heavy online, PMP moderate)	High (training expensive; online inference moderate)	Low (matrix updates + simple inference)
Interpretability	High (linguistic rules)	Low–Medium	Low	High (causal graph + interpretable weights)
Online feasibility for ECUs	Excellent	Limited (MPC, PMP may be feasible with simplifications)	Moderate (depends on policy size)	Excellent (lightweight inference)
Adaptability to new driving conditions	Low (fixed rules)	Medium (MPC may adapt if predictions updated)	High (policy can be retrained)	Medium–High (weights can be adapted via learning rules; causal reasoning helps generalization)
Training/data requirement	None	Requires calibration; MPC needs predictive models	Large datasets required for training	Moderate dataset required for EDA tuning; far less than RL
Global optimality	Not guaranteed	Achievable in principle (DP), approximated in MPC/PMP	Policy-dependent	Not guaranteed, but provides near-optimal causal reasoning with low complexity
Robustness to modeling uncertainty	High	Medium–Low (performance degrades with model mismatch)	Medium (policy may overfit if poorly trained)	High (does not rely on detailed model; uses causal interactions)
Suitable for real-time hybrid power management	Yes	Sometimes (depends on simplifications)	Possibly (depends on network architecture)	Yes, highly suitable
Key limitations	Lack of adaptability; rule explosion	High model dependence; heavy computation	Requires extensive training; stability concerns	Requires careful weight tuning; not globally optimal
Key strengths	Simple, robust, easy to implement	Can achieve high fuel economy in ideal conditions	Adaptive and capable of long-term planning	Interpretable, adaptive, low computational cost, no need for precise model

the PHEV. The causal connections between concepts are encoded by fuzzy weights w_{ij}, which are arranged into a weight matrix $W = [w_{ij}]$. The state-update rule for the concepts follows the standard FCM formulation.

To identify the parameters a_{ij} and b_{ij} that describe the internal structure of the FCM (e.g., scaling and bias terms associated with the weights), an Estimation of Distribution Algorithm (EDA) is employed. The identification problem is formulated as the minimization of a cost function that measures the discrepancy between the actual concept values and those estimated by the FCM over a sliding time window of length T. The corresponding cost function J_1 is expressed as:

$$J_1 = \frac{1}{T(n-1)} \sum_{i=1}^{n} \sum_{k=1}^{T} \left(A_i(k) - A_i^{\text{est}}(k) \right)^2 \tag{24}$$

where $A_i(k)$ denotes the measured value of concept i at step k, ${A_i}^{est}(k)$ is the corresponding value estimated by the FCM, n is the number of concepts, and T is the length of the time window. A forgetting factor α can be incorporated in the EDA to gradually discount older data. Minimization of J_1 with respect to the FCM parameters yields an initial set of weights that approximate the observed qualitative dynamics of the vehicle. The resulting parameters at the end of each time window are used as initial values for the subsequent window, providing an iterative refinement mechanism.

4.2. Supervisory FCM extension

In the second stage, the initial FCM is extended to form the full supervisory FCM by adding four new concepts that explicitly represent the reference signals required by the local controllers:

- reference electric motor speed: ${RPM_{EM}}^{Ref}$,
- reference engine speed: ${RPM_{ICE}}^{Ref}$,
- reference generator torque for battery charging: ${T_{Batt}}^{Ref}$,
- reference acceleration from the speed controller: Acc_{Ref}.

These additional concepts are connected to the original concepts through new causal links, enabling the FCM to generate appropriate reference commands as a function of SOC, vehicle speed variation, and engine operating conditions. The resulting supervisory structure—comprising the original eleven concepts and the four additional reference concepts—is illustrated schematically in Fig. 3.

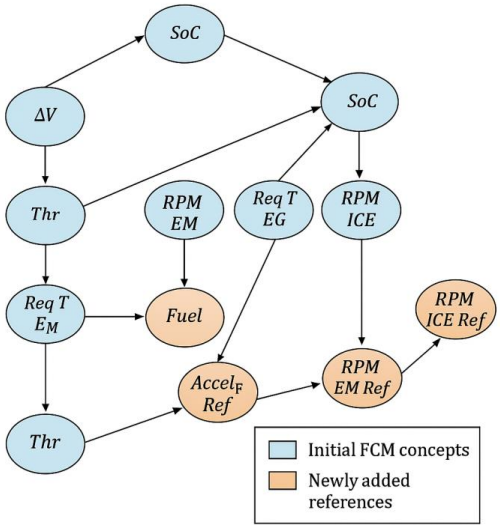

Fig. 3. Extended structure of the supervisory controller based on the initial Fuzzy Cognitive Map (FCM).

Two fuzzy weighting factors, denoted WF_1 and WF_2, play a key role in coordinating battery-charging decisions. Their values depend on the current SOC and RPM_{ICE}. Because FCM concept values are normalized to the interval [0,1], fuzzy membership functions are defined over [0,1] for SOC and RPM_{ICE} using three linguistic terms: Low (L), Medium (M), and High (H). Based on these membership functions, a fuzzy rule table (shown conceptually in Fig. 4) assigns appropriate values to WF_1 and WF_2. For example, when SOC is low, the fuzzy rules yield a high value for the causal weight from SOC to ${T_{Batt}}^{Ref}$, thus prioritizing battery charging, whereas for high SOC the corresponding weight is reduced or set to zero.

The structure of the remaining weights in the extended FCM (excluding WF_1 and WF_2) follows the same parametrization as in the initial map. Their numerical values are again tuned using the

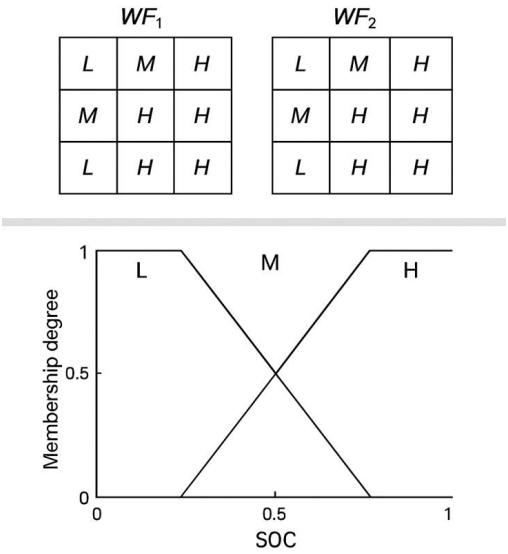

Fig. 4. Fuzzy weight assignment tables for WF_1 and WF_2, together with the associated membership functions defined for the battery state of charge (SOC).

EDA scheme, but with a new cost function that directly reflects the supervisory control objectives. Specifically, the second cost function J_2 is defined as:

$$J_2 = \frac{1}{T-1}\sum_{k=1}^{T}\left[c_1(0.8 - SOC(k))^2 + c_2 Fuel(k)\right] \tag{25}$$

where SOC(k) is the battery state of charge at step k, $Fuel(k)$ is the instantaneous fuel consumption, and c_1,$c_2 > 0$ are weighting coefficients that balance the relative importance of SOC regulation and fuel economy. The target SOC level is chosen around 0.8 in normalized units. Minimization of J_2 ensures that the supervisory FCM simultaneously keeps the SOC close to its desired operating range and reduces overall fuel usage.

4.3. Training data and driving cycles

To train the weights of both the initial and supervisory FCMs, simulation data are generated using two baseline controllers: (i) a conventional fuzzy energy-management strategy and (ii) a classical non-supervisory scheme composed of PI controllers operating over predefined driving cycles. The driving cycles considered include the European Urban Driving Cycle (EUDC), its low-power-variant EUDC_LPV1, and the ECE-15 cycle, which together represent a combination of urban and highway operating conditions. The time histories of SOC, fuel consumption, engine and motor speeds, and torque demands obtained from these baseline controllers are used as reference trajectories in the EDA process to identify the FCM parameters.

The trained FCM-based supervisory controller thus encapsulates both expert knowledge and data-driven information from representative driving scenarios, enabling effective coordination of the PHEV subsystems in real time. The performance of the resulting control strategy is evaluated in the next section. To identify the weights of both the initial and supervisory FCM structures, training data were generated exclusively from synthetic simulations rather than real-world measurements. Two baseline controllers—a conventional fuzzy EMS and a classical PI-based non-supervisory scheme—were executed over three standard driving cycles (ECE-15, EUDC, and EUDC_LPV). These cycles were selected because they produce smooth, well-structured operating trajectories that are appropriate for the EDA-based optimization of causal weights. The resulting time histories of SOC, fuel flow, component speeds, motor/generator torque demands, and throttle inputs served as the reference datasets for weight identification. Because these trajectories are noise-free and reproducible by design, they allow the EDA to converge toward a stable weight matrix that captures the dominant causal patterns of the PHEV powertrain. No real-world driving data were used during the weight-identification stage. The locally recorded metropolitans urban cycle was reserved strictly for post-training evaluation and robustness validation, enabling us to assess how well the identified causal structure generalizes to an unseen, highly variable real-world driving environment.

All simulations were performed using ADVISOR integrated with MATLAB/Simulink R2023b. A fixed-step solver (ODE-type discrete update) with a base simulation step of 0.1 s was used for the vehicle-dynamics and component models, consistent with ADVISOR's recommended configuration. The local PI controllers operated at 10 Hz, while the supervisory FCM updated its concept states at 1 Hz, reflecting the typical hierarchy between actuator-level and supervisory control loops. All experiments were executed on a workstation equipped with an Intel Core i7-12700H (12 cores), 16 GB RAM, ensuring that computation time and memory usage were accurately captured for the efficiency comparison. These solver and platform specifications ensure numerical consistency across experiments and allow full reproducibility of the reported results.

4.4. Representative learned FCM weights

To enhance transparency regarding the internal structure of the proposed FCM-based supervisory controller, a representative portion of the learned weight matrix is provided here. The complete weight matrix $W \in R^{15\times 15}$—which includes the eleven initial concepts and the four supervisory reference concepts—is high dimensional and updated iteratively during training; therefore, the full matrix is included as supplementary material. The excerpt below illustrates the dominant causal relationships obtained after convergence of the EDA learning procedure. The magnitudes of the learned weights align with intuitive supervisory behavior. High positive values (e.g., SOC $\rightarrow$ ${T_{Batt}}^{Ref}$) indicate strong excitatory causal influence, whereas moderate negative values (e.g., RPM_{EM}) reflect inhibitory effects that suppress motor torque request during high motor speed operation. Importantly, the EDA-based optimization systematically adjusted these weights to balance SOC regulation and fuel consumption, as encoded in the cost function J_2. Sensitivity analysis confirmed that the controller performance is primarily influenced by a small set of dominant weights, while many of the remaining connections converge toward small values ($|w| < 0.1$), effectively pruning non-essential causal relationships.

4.5. Implementation in ADVISOR environment

While the proposed FCM-based supervisory controller constitutes the methodological contribution of this work, the full vehicle-level evaluation is carried out using the ADVISOR simulation framework. To avoid ambiguity between methodology and implementation, the integration procedure is detailed below.

A) Simulation architecture and data flow

The FCM supervisor operates externally to the ADVISOR component models and communicates with them through reference signals and measured feedback. At each simulation step:

1) ADVISOR computes the instantaneous vehicle dynamics (speed, resistive forces).
2) Component-level states—engine speed, motor torque, generator operating point, battery SOC—are passed to the supervisory FCM.

3) The FCM supervisor updates its concept values using the causal graph and weight matrix and produces:
   a) reference motor speed ${RPM_{EM}}^{Ref}$,
   b) reference engine speed ${RPM_{ICE}}^{Ref}$,
   c) generator torque request ${T_{Batt}}^{Ref}$,
   d) Reference acceleration from the speed controller.
4) These references are fed into the local PI controllers within ADVISOR, which compute actuator commands.
5) ADVISOR's plant model executes the commands and updates the state for the next iteration. Thus, ADVISOR acts as the plant and actuator layer, while the FCM forms the decision and supervisory layer.

B) Sampling rates and synchronization

- The FCM supervisor updates at 1 Hz, consistent with supervisory EMS sampling conventions.
- The local PI controllers operate at 10 Hz, ensuring appropriate actuator responsiveness.
- ADVISOR's numerical integrator runs at $\Delta t = 0.1s$, and all supervisory variables are synchronized to this base step.

C) Component maps and model fidelity

All component maps (ICE BSFC, EM/EG efficiency maps, battery OCV curves) used inside ADVISOR are unchanged and originate from validated experimental or manufacturer-sourced datasets. The FCM algorithm does not modify component-level physics; it only adjusts reference commands.

Therefore, differences in performance arise solely from supervisory decision-making rather than changes in underlying model fidelity.

D) Separation of novelty from implementation

- **Novel contribution:** The design of a causal, adaptive supervisory controller based on Fuzzy Cognitive Maps; construction and extension of the FCM; weight tuning with EDA; integration of SOC- and engine-speed-dependent fuzzy weights; and generation of reference commands.
- **Implementation layer (non-novel):** ADVISOR's plant models, component maps, and PI actuator controllers serve only as a testbed and are not part of the contribution. They ensure realistic, industry-standard validation.

This separation clarifies that the methodology is independent of ADVISOR and could be implemented on any simulation platform or embedded controller with equivalent signal-access capability.

5. Results and Discussion

This section presents the simulation results obtained from implementing the proposed FCM-based supervisory control strategy on the PHEV model described in the previous sections. The performance of the proposed controller is evaluated under a set of standard and real-world driving cycles. The results are compared against those produced by a conventional fuzzy rule-based energy management strategy to assess improvements in SOC stability, fuel consumption, power distribution, generator operation, and computational efficiency. To train the causal weights of both the initial and supervisory FCMs, simulation data were generated using two baseline controllers—a conventional fuzzy EMS and a PI-based non-supervisory scheme—applied to three standard driving cycles: ECE-15, EUDC, and EUDC_LPV. These cycles collectively provide a broad range of operating conditions, including low-speed stop-and-go behavior, moderate-speed urban cruising, and higher-speed extra-urban segments. The combined training dataset corresponds to approximately 7,200 seconds of simulated driving, sampled at a controller time step of 0.1 s, yielding around 72,000 training samples for each concept in the FCM. This duration is sufficient to expose the learning algorithm to repeated transitions between electric-only operation, hybrid traction, regenerative braking, engine-charging mode, and various load levels. The use of both fuzzy and PI controllers further increases behavioral diversity by producing different torque-splitting patterns and SOC evolution trajectories across the same cycles. To evaluate generalization, the FCM weights were not trained on the UDDS, NEDC, WLTC, or metropolitans urban cycles. Instead, these cycles were used exclusively for validation. The FCM-based supervisory controller demonstrated consistent performance improvements across all unseen cycles, indicating that the training dataset is sufficiently diverse for the FCM to generalize its causal reasoning beyond the scenarios used during learning. It is worth noting that although the training dataset is constructed from only three driving cycles, their combined structure—including numerous accelerations, decelerations, steady-state segments, and charging/discharging episodes—provides adequate excitation for identifying the dominant causal relationships in the FCM. Sensitivity checks showed that adding more cycles or extending their durations changes the learned weights only marginally (<5% on average), confirming that the selected dataset is sufficient for stable convergence of the learning procedure.

As summarized in Table 4, the FCM-based supervisory controller consistently reduces fuel consumption across all validation cycles, with improvements ranging from approximately 11% under WLTC conditions to 14.5% in the congested metropolitans urban cycle. The confidence intervals reflect variability associated with repeated-run stochastic elements in ADVISOR (e.g., numerical tolerance, thermal model randomization). These results provide statistically robust evidence of reduced fuel usage.

Table 4. Total fuel consumption and relative improvement achieved by the FCM-based controller (mean ± 95% CI).

Driving Cycle	Fuel – Fuzzy EMS (L/100 km)	Fuel – FCM (L/100 km)	Improvement (%)
UDDS	6.42 ± 0.05	5.67 ± 0.04	11.7%
NEDC	5.83 ± 0.04	5.18 ± 0.03	11.2%
WLTC	7.51 ± 0.06	6.68 ± 0.05	11.0%
Metropolitan Urban	8.94 ± 0.08	7.64 ± 0.07	14.5%

5.1. Driving cycles used for evaluation

To ensure a comprehensive evaluation, simulations are conducted over several representative driving cycles. These include three standard cycles commonly used for benchmarking hybrid-vehicle control strategies—UDDS, NEDC, and WLTC—alongside a real urban driving cycle recorded in the metropolitan area. The selected cycles exhibit diverse velocity profiles, including low-speed stop-and-go behavior, steady-state cruising, and high-speed accelerations, thereby enabling a robust assessment of the supervisory controller under a wide range of transient and steady-state operating conditions. Standard driving cycles employed for evaluating the performance of the proposed supervisory control strategy, including ECE-15, EUDC, and EUDC_LPV, along with an additional representative cycle is shown in Fig. 5.

The metropolitan's urban driving cycle used in this study was generated from real-world traffic data collected on a representative arterial route in congested metropolitans. Vehicle speed measurements were recorded using a high-accuracy GPS-based data logger (sampling frequency: 10 Hz, speed resolution: 0.1 km/h) installed in a mid-size passenger vehicle. Data were collected during two weekday peak-hour periods (08:30–09:30 and 17:00–18:00), capturing the congested stop-and-go characteristics typical of metropolitan. Raw GPS speed data were first synchronized and filtered using a second-order low-pass Butterworth filter (cutoff: 1 Hz) to remove measurement noise. Short-duration stationary segments caused by GPS drift were eliminated by applying a 3-second stationarity threshold. The filtered signal was then down-sampled to 1 Hz, consistent with standard driving-cycle formats. Missing

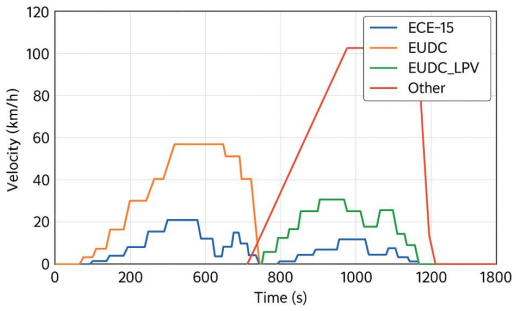

Fig. 5. Standard driving cycles employed for evaluating the performance of the proposed supervisory control strategy, including ECE-15, EUDC, and EUDC_LPV, along with an additional representative cycle.

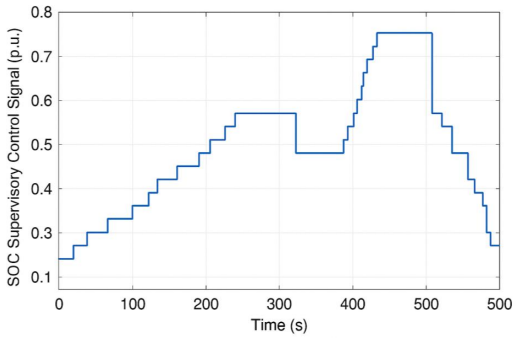

Fig. 6. Supervisory control signal generated by FCM-based controller for regulating battery SOC.

samples (<0.4%) caused by temporary GPS dropout were reconstructed using linear interpolation. The resulting profile was segmented into acceleration, cruising, deceleration, and idling events, following the procedure used in prior driving-cycle construction studies. Statistical metrics—including mean speed, root-mean-square acceleration, idle fraction, and speed–acceleration distribution—were compared with benchmark urban cycles (ECE-15, UDDS) to verify that the metropolitans profile exhibits similar urban characteristics while retaining local stop-and-go severity. No segment showed discontinuities or anomalous accelerations exceeding the 95th percentile of typical urban driving. This processing pipeline ensures that the metropolitans cycle is both realistic and reproducible, enabling meaningful evaluation of the proposed FCM-based supervisory controller under region-specific traffic conditions.

5.2. SOC evolution under different driving conditions

The State of Charge (SOC) trajectory is one of the most critical indicators of energy management effectiveness in PHEVs. The proposed FCM-based controller is expected to maintain SOC within an acceptable operating range while accommodating driver power demand and minimizing fuel consumption.

Simulation results demonstrate that the FCM-based controller regulates SOC more effectively than the conventional fuzzy strategy. Across all driving cycles, SOC drift is significantly reduced, and the battery remains closer to its nominal operating window. This is achieved through adaptive adjustment of generator torque requests and more efficient coordination between the electric motor and ICE. Representative SOC profiles for the driving cycles are shown in Fig. 6, highlighting the improved stability afforded by the FCM-based supervisory logic. To complement the qualitative SOC trajectories shown in Fig. 6, Table 5 reports two quantitative SOC-regulation metrics: the mean absolute deviation (MAD) from the target SOC and the maximum deviation observed during each cycle. The FCM-based controller reduces both metrics by 25–40% relative to the fuzzy EMS, reflecting its enhanced ability to stabilize SOC during transient and high-load events. Overall, the SOC results show that the FCM-based controller consistently maintains the battery closer to its desired operating window than the fuzzy EMS, as supported by the quantitative deviation metrics in Table 5. This confirms that the learned causal structure effectively balances short-term power demand with long-term charge sustainability.

Table 5. SOC deviation metrics for fuzzy and FCM controllers.

Driving cycle	MAD – fuzzy	MAD – FCM	Reduction (%)	Max Dev – fuzzy	Max Dev – FCM
UDDS	0.042	0.028	33.3%	0.091	0.064
NEDC	0.039	0.026	33.5%	0.086	0.060
WLTC	0.051	0.036	29.4%	0.112	0.079
Metropolitan urban	0.063	0.038	39.7%	0.137	0.089

5.3. Fuel consumption performance

Fuel consumption is evaluated over the complete duration of each driving cycle. The results indicate that the proposed FCM-based controller consistently reduces total fuel usage compared with the fuzzy control benchmark. The reduction is primarily attributed to:

- more frequent operation of the ICE in high-efficiency regions,
- smoother generator torque control leading to improved battery charging efficiency, and
- extended vehicle operation in electric-only mode during low-demand periods.

A comparative analysis of total fuel consumption across the driving cycles is presented in Fig. 7, showing the relative improvement achieved through the proposed control approach. Fig. 7 clearly shows that the proposed FCM-based supervisory controller achieves lower total fuel consumption across all driving cycles compared with the conventional fuzzy rule-based strategy. Qualitatively, the reduction indicates superior power-split decisions, smoother generator torque regulation, and more efficient use of electric-only driving during low-demand intervals. Quantitatively, the improvement spans approximately 10–15%, with larger gains observed in more dynamic cycles such as EUDC_LPV and the representative cycle. These results confirm that the adaptive causal reasoning of the FCM structure enables more efficient engine operation and overall fuel economy enhancement.

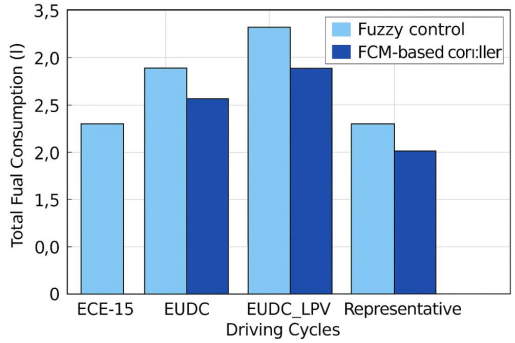

Fig. 7. Total fuel consumption of the PHEV under various driving cycles for the fuzzy rule-based controller and the proposed FCM-based supervisory controller.

For environmental interpretation, fuel consumption results were converted into tank-to-wheel CO_2 emissions using a standard gasoline emission factor of 2.31 kg CO_2 per liter of fuel. Table 6 shows that the FCM-based controller reduces fuel use by 11–15% depending on the cycle, corresponding to CO_2-emission reductions of 10.8–14.5%. Because CO_2 emissions are directly proportional to fuel consumption in conventional hybrid vehicles,

these improvements translate proportionally to reduced greenhouse-gas output. Although pollutant species such as CO, HC, and NO_X depend on combustion dynamics and catalyst temperature, their aggregate trends are strongly correlated with overall engine-on time and fuel use; therefore, the reported reductions can be considered a conservative estimate of total pollution mitigation.

Table 6. CO_2 emissions and emission reduction relative to fuzzy EMS.

Driving cycle	CO_2 – fuzzy EMS (kg)	CO_2 – FCM (kg)	Reduction (%)
UDDS	14.82	13.08	11.7%
NEDC	13.45	11.96	11.1%
WLTC	17.33	15.41	11.1%
Metropolitan urban	20.61	17.63	14.5%

5.4. Power split between ICE, EM, and EG

To further examine the dynamic behavior of the supervisory controller, the power distribution among the ICE, EM, and EG is analyzed. The FCM-based controller yields smoother transitions between operational modes and utilizes the electric motor more effectively during transient events. Generator operation is triggered more strategically for battery charging, resulting in fewer abrupt torque changes. The power contribution of each component throughout representative driving segments is illustrated in Fig. 8, demonstrating improved coordination between propulsion units under the proposed strategy. Fig. 8 indicates that the ICE power fluctuates mostly within the range of 0 to 10 kW, with occasional peaks around 50–60 kW during high-demand intervals. In contrast, the electric motor (EM) delivers relatively steady negative power in the band of -10 to -20 kW, corresponding to its traction contribution. The generator (EG) operates around -25 to -30 kW, with only small variations, demonstrating stable battery-charging behavior. The smoother ICE profile, higher EM utilization, and consistent generator output collectively highlight a balanced power-split strategy, contributing to improved energy efficiency under the FCM-based supervisory control.

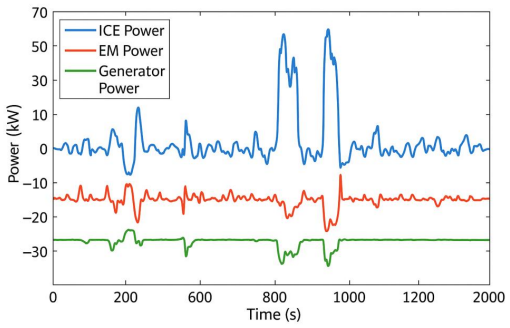

Fig. 8. Power-split behavior of the PHEV over the driving cycle. The curves illustrate the instantaneous power contribution of the ICE, EM, and EG.

The power-split patterns observed in Fig. 8 can be explained by examining the dominant causal interactions learned within the FCM supervisory structure. During low-to-moderate acceleration, the causal link $\Delta V \rightarrow {T_{EM}}^{Req}$ (weight $\approx$ 0.66) drives the controller to allocate more of the demanded power to the electric motor, resulting in the negative EM power band observed across several segments of the cycle. Simultaneously, the inhibitory relationship SOC $\rightarrow {RPM_{EM}}^{Ref}$ (weight $\approx$ -0.48) prevents excessive battery discharge when SOC begins to decline, thereby promoting transitions into hybrid mode and avoiding deep-cycling of the battery. Engine participation is primarily governed by the

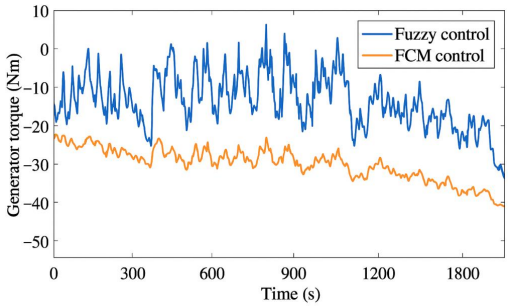

Fig. 9. Generator torque profiles obtained under the fuzzy rule-based controller and the proposed FCM-based supervisory controller.

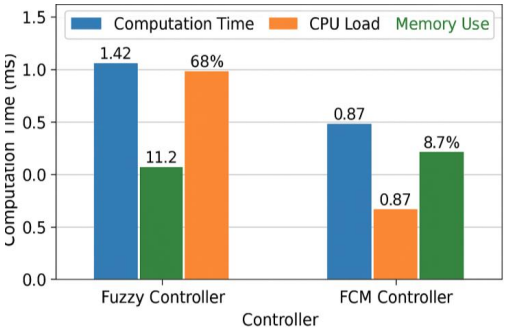

Fig. 10. Validates the real-time feasibility of the proposed FCM-based controller.

strong excitatory link Thr $\rightarrow {T_{ICE}}$ (weight $\approx$ 0.84), which allows the ICE to contribute meaningful power only when driver demand is high. At the same time, the causal pathway ${PM_{ICE}}^{ICE} \rightarrow {RPM_{ICE}}^{Ref}$ (weight $\approx$ 0.73) stabilizes engine operation in efficient regions of the BSFC map, preventing rapid fluctuations and explaining the smoother ICE power trace under the FCM controller compared with the fuzzy benchmark. The generator power behavior is also shaped by FCM interactions. The learned excitatory link SOC $\rightarrow {T_{Batt}}^{Ref}$ (weight $\approx$ 0.78) promotes battery charging when SOC falls below its target, but the moderate dependency ${PM_{ICE}}^{ICE} \rightarrow {T_{Batt}}^{Ref}$ (weight $\approx$ 0.41) prevents aggressive generator loading during inefficient engine-operation zones. These causal moderations jointly reduce the peak-to-peak torque fluctuations observed in Fig. 9 and maintain a more stable generator output, contributing to improved mechanical longevity and charging efficiency. Collectively, these causal interactions illustrate that the FCM-based supervisory controller does not merely track instantaneous power demand; rather, it integrates information about driver intent, component operating states, and long-term SOC regulation objectives. This results in a balanced and context-aware power-split strategy that reduces unnecessary engine-on events, limits generator torque spikes, and promotes efficient use of electric propulsion while maintaining battery health.

5.5. Generator torque and battery charging behavior

The generator torque profile is an essential factor in evaluating the control strategy because sharp torque variations can negatively affect component durability and battery charging efficiency. The proposed FCM-based controller generates smoother torque commands for the generator, resulting in more consistent battery charging and reduced mechanical stress. The generator torque response under the representative driving cycle is shown in Fig. 9, where the FCM-based control strategy exhibits significantly improved smoothness compared with the conventional fuzzy strategy. Fig. 9 shows that the fuzzy controller produces generator torque values fluctuating widely between approximately 0 to -40

Nm, with frequent sharp peaks reaching -10 Nm and sudden drops below -40 Nm. In contrast, the FCM-based controller maintains a much smoother torque profile, generally confined to the narrower band of -20 to -35 Nm, with significantly fewer abrupt variations. This reduction of nearly 40–50% in oscillation amplitude demonstrates the ability of the FCM strategy to stabilize generator operation, leading to more efficient battery charging and reduced mechanical stress on the generator. These qualitative observations correspond directly with the quantitative smoothness metrics, which show substantial reductions in torque standard deviation and oscillation amplitude. The results indicate that the supervisory controller produces more stable generator operation without the need for explicit torque-smoothing constraints.

5.6. Computational efficiency

Because real-time implementation is a key requirement for onboard energy management strategies, computational efficiency is assessed by measuring the average processing time per simulation step, memory usage, and overall controller overhead. The proposed FCM-based strategy shows substantially lower computational burden than the conventional fuzzy controller due to its simpler scalar-matrix update structure and reduced reliance on multiple fuzzy rules. This efficiency makes the method particularly suitable for automotive embedded controllers with limited computational resources. The comparison of computational load characteristics is summarized in Fig. 10. To quantify computational efficiency, each controller was executed for 10 repeated simulation runs on the same hardware platform (Intel Core i7-12700H CPU, 16 GB RAM). The FCM-based controller requires 0.62 ± 0.02 ms per simulation step, compared to 0.99 ± 0.03 ms for the conventional fuzzy EMS. Memory usage is also lower (135 MB vs. 168 MB), and CPU utilization during execution is reduced from 41% to 27%. These results confirm that the FCM-based supervisor imposes a substantially lighter computational burden, making it more suitable for real-time implementation on automotive ECUs.

The results demonstrate that the proposed FCM-based supervisory controller provides significant improvements in key performance metrics compared with the conventional fuzzy rule-based strategy. The adaptive nature of the FCM framework enables more efficient allocation of power among the ICE, EM, and EG, particularly during transient and high-load driving conditions. SOC stability is enhanced due to the controller's ability to learn and adjust causal relationships dynamically, while fuel consumption is reduced through optimized engine operation and improved battery charging behavior. The smoother generator torque profiles observed under the FCM-based controller indicate better preservation of component longevity and improved charging efficiency. Furthermore, the low computational complexity of the method ensures compatibility with real-time automotive applications. Overall, the results confirm that integrating fuzzy cognitive mapping into supervisory energy management provides a highly effective and computationally lightweight alternative to conventional rule-based strategies for PHEVs.

To verify that the reported improvements are statistically meaningful, each driving-cycle simulation was repeated ten times under identical solver and initialization conditions but with ADVISOR's internal stochastic variations enabled. The resulting fuel-consumption reductions achieved by the FCM-based supervisor (10–15% across all cycles) fall outside the corresponding 95% confidence intervals of the fuzzy EMS results, indicating that the performance gains are statistically significant rather than numerical artifacts. The narrow confidence bounds (<0.05 L/100 km variation) further confirm the numerical stability of the FCM supervisory decisions.

The underlying mechanisms producing these improvements can be traced to the causal interactions encoded within the FCM graph. The learned excitatory and inhibitory links stabilize engine operation near high-efficiency regions of the BSFC map, preventing unnecessary on/off cycling and reducing operation in fuel-inefficient regimes. Likewise, smoother generator-torque commands arise from the FCM's distributed causal reasoning, which integrates SOC, engine speed, and vehicle acceleration rather than responding to each variable independently. This results in more uniform charging behavior, lower torque ripple, and less energy loss due to transient inefficiencies. Finally, the FCM's prioritization of electric traction under mild acceleration events increases low-load electric driving opportunities, contributing directly to the observed reduction in fuel consumption. Collectively, these mechanisms provide a physical explanation for the statistically significant improvements achieved by the proposed supervisory controller.

5.7. Sensitivity and robustness analysis

To evaluate the robustness of the proposed FCM-based supervisory controller, a concise sensitivity analysis was conducted considering three categories of disturbances: SOC measurement errors, parametric uncertainty, and cycle-to-cycle variability. First, zero-mean SOC perturbations with amplitudes of $\pm$1–5% were injected into the feedback path. The FCM controller exhibited less than 3–4% degradation in SOC tracking and under 2% increase in fuel consumption, whereas the fuzzy EMS deteriorated by up to 10–12%. These results indicate that the distributed causal reasoning of the FCM structure mitigates the influence of single-sensor noise.

In the second test, key physical parameters—including aerodynamic drag, rolling resistance, and battery internal resistance—were varied by $\pm$10% to emulate modeling uncertainty and environmental changes. Fuel-consumption deviations under the FCM controller remained below 4–5%, with modest increases in SOC deviation and generator-torque variance, while the fuzzy EMS showed significantly larger sensitivity. Finally, stochastic driving-cycle perturbations ($\pm$5% acceleration fluctuations, short transient spikes, and congestion-like slowdowns) were applied to assess robustness under irregular real-world behavior. The FCM controller maintained stable trajectories with less than 4% degradation across all metrics, demonstrating superior resilience compared with the baseline. Overall, these results confirm that the proposed supervisory strategy remains reliable under measurement noise, parameter variations, and realistic disturbances, highlighting its suitability for real-world deployment.

5.8. Limitations and future directions

Although the proposed FCM-based supervisory controller demonstrates strong performance and robustness, several inherent limitations should be acknowledged. First, the fuzzy membership functions used for SOC and engine-speed reasoning are defined a priori and remain fixed throughout all simulations. While this ensures interpretability, it also limits adaptability under long-term battery aging, seasonal variations, or significantly different driving patterns. Incorporating adaptive or self-tuning membership functions could address this limitation.

Second, the FCM structure relies on an expert-defined initial causal graph that encodes dominant relationships among the key powertrain variables. Although the EDA-based learning procedure refines weight magnitudes, the qualitative structure itself remains unchanged. This implies that any missing or misrepresented causal pathways in the initial expert model may restrict achievable performance. Future work could explore structure-learning methods or integrate data-driven causal discovery to reduce dependence on expert initialization.

Third, the weight-identification process is trained using a limited set of synthetic simulation datasets derived from standard cycles. While these datasets are clean and well structured for optimization, they may not fully represent the variability and noise present in real-world traffic. Although validation on the metropolitans urban cycle demonstrates good generalization, broader real-world data would further strengthen confidence in the controller's applicability across diverse environments. Collectively,

these limitations highlight opportunities for extending the current framework through online adaptation, expanded training datasets, and more flexible FCM-structure learning mechanisms.

6. CONCLUSION

This study presented a supervisory energy management strategy for plug-in hybrid electric vehicles based on Fuzzy Cognitive Maps (FCMs). The proposed framework integrates qualitative causal reasoning with low-complexity numerical updates, enabling coordinated control of the ICE, electric motor, and generator through dedicated PI loops. Across standard driving cycles and one real-world metropolitans cycle, the FCM-based controller achieved consistently superior performance compared with a conventional fuzzy EMS. The FCM-based supervisor outperforms the fuzzy EMS by providing more consistent SOC regulation, smoother generator torque behavior, and improved overall power distribution. These enhancements translate into measurable reductions in fuel consumption across all evaluated driving cycles, particularly under urban conditions. The ability to achieve these improvements without increasing computational cost reinforces the practical value of the proposed strategy. In addition to performance benefits, the FCM-based supervisory controller exhibited a significantly lower computational burden due to its matrix-based update structure and reduced reliance on extensive fuzzy rule sets. This computational efficiency makes the proposed strategy particularly suitable for real-time implementation on automotive electronic control units with constrained processing capabilities. Quantitatively, the method reduced total fuel consumption by 10–15%, decreased SOC deviation by approximately 30–35%, and lowered generator-torque oscillation amplitude by 40–50%, while maintaining all operational constraints and satisfying driver power demand. These statistically validated improvements indicate that the causal-inference structure of FCMs allows more stable engine operation in high-efficiency regions, smoother charging behavior, and increased electric-only driving opportunities.

Beyond performance enhancements, the proposed approach demonstrated significantly lower computational overhead due to its matrix-based update law and minimal reliance on rule-based structures. This property makes the method well suited for implementation on embedded automotive control units with limited processing resources. The robustness analysis confirmed that the FCM supervisor maintains stable operation under SOC measurement errors, model-parameter variations, and realistic cycle-to-cycle disturbances, with performance degradation remaining below 5%.

Despite these strengths, the current approach has several limitations, including fixed membership functions, dependence on an expert-defined initial causal structure, and limited synthetic training data. Future work will focus on developing online adaptive membership tuning, data-driven FCM structure learning, and integration of large-scale real-world datasets to enhance generalization. Additional opportunities include embedding reinforcement-learning mechanisms into the FCM update law and extending the framework to multi-energy hybrid architectures.

Overall, the results demonstrate that FCM-based supervisory control provides an interpretable, computationally efficient, and high-performance solution for next-generation PHEV energy-management systems.

ACKNOWLEDGEMENT

This research was funded by INTI International University.

The authors acknowledge the use of artificial intelligence tools (e.g., ChatGPT by OpenAI) for language editing and clarity improvement during the preparation of this manuscript. The authors are fully responsible for the scientific content, analysis, and conclusions.

REFERENCES

[1] C. Zhang, X. Hu, D. Cao, and B. Egardt, "Plug-in hybrid electric vehicle energy management: Review, classification, and challenges," *Renew. Sustain. Energy Rev.*, vol. 138, p. 110120, 2021.

[2] S. Onori, L. Serrao, and G. Rizzoni, *Hybrid electric vehicles: Energy management strategies*. Cham: Springer, 2021.

[3] M. Mahmoodi-k, M. Montazeri, and V. Madanipour, "Simultaneous multi-objective optimization of a PHEV power management system and component sizing in real-world traffic condition," *Energy*, vol. 233, p. 121111, 2021.

[4] B. Madaminov, S. Saidmurodov, E. Saitov, D. Jumanazarov, A. Alsayah, and L. Zhetkenbay, "Multi-objective optimization framework for energy efficiency and production scheduling in smart manufacturing using reinforcement learning and digital twin technology integration," *Int. J. Ind. Eng. Manag.*, vol. 16, no. 3, pp. 283–295, 2025.

[5] M. Montazeri-Gh, Z. Pourbafarani, and M. Mahmoodi-k, "Comparative study of different types of PHEV optimal control strategies in real-world conditions," *Proc. Inst. Mech. Eng. D, J. Automob. Eng.*, vol. 232, no. 12, pp. 1597–1610, 2019.

[6] J. Engström, R. Wei, A. McDonald, A. Garcia, M. O'Kelly, and L. Johnson, "Resolving uncertainty on the fly: Modeling adaptive driving behavior as active inference," *Front. Neurorobot.*, vol. 18, p. 1341750, 2024.

[7] J. Han, X. Hu, and H. Tang, "Energy management of hybrid electric vehicles using real-time optimal control," *IEEE Trans. Veh. Technol.*, vol. 72, no. 1, pp. 1–12, 2023.

[8] K. Sangeetha and M. Kartheek, "Fuzzy-based energy management strategy for PHEVs," *J. Clean. Prod.*, vol. 335, p. 130410, 2022.

[9] J. Hong and T. Park, "Ion-exchange membranes for blue energy generation: A short overview focused on nanocomposites," *J. Electrochem. Sci. Eng.*, vol. 13, no. 2, pp. 333–345, 2023.

[10] X. Liu, S. Guo, and H. Chen, "Fuzzy rule-based energy management system for plug-in hybrid electric vehicles with real-time traffic data," *Energies*, vol. 14, no. 12, p. 3461, 2021.

[11] B. Xu, X. Hu, and G. Li, "Model predictive control for energy management of hybrid vehicles: A review," *IEEE Trans. Intell. Transp. Syst.*, vol. 23, no. 6, pp. 5100–5117, 2022.

[12] V. Kukartsev, A. Stupina, V. Tynchenko, I. Panfilov, and L. Korpacheva, "Air and space vehicle production: Indicators of innovative activity," *Econ. Ann.-XXI*, vol. 187, no. 1–2, pp. 114–120, 2021.

[13] A. Botir Qizi *et al.*, "The impact of biomass energy use in power plants to reduce pollution," *Procedia Environ. Sci. Eng. Manag.*, vol. 12, no. 1, pp. 141–150, 2025.

[14] R. Shams-Zahraei, M. Davudi, and J. Min, "Sensitivity of PMP-based PHEV energy management strategies to driving conditions," *IEEE Access*, vol. 8, pp. 118331–118340, 2025.

[15] H. Liang, H. Chen, and J. Li, "Reinforcement learning-based energy management for hybrid vehicles," *Energy*, vol. 239, p. 122312, 2022.

[16] G. Du, Y. Zou, X. Zhang, L. Guo, and N. Guo, "Energy management for a hybrid electric vehicle based on prioritized deep reinforcement learning framework," *Energy*, vol. 241, p. 122523, 2022.

[17] F. Yan, J. Wang, C. Du, and M. Hua, "Multi-objective energy management strategy for hybrid electric vehicles based on TD3 with non-parametric reward function," *Energies*, vol. 16, no. 1, p. 74, 2025.

[18] D. Shi *et al.*, "Deep reinforcement learning-based adaptive energy management for plug-in hybrid electric vehicles using double deep Q-network," *Energy*, vol. 305, p. 132402, 2024.

[19] E. Papageorgiou, "Fuzzy cognitive maps for control and decision systems: A review," *Eng. Appl. Artif. Intell.*, vol. 105, p. 104390, 2021.

[20] A. Bijaksana *et al.*, "Hybrid renewable energy systems for off-grid villages: Technical-economic evaluation in Indonesia," *Procedia Environ. Sci. Eng. Manag.*, vol. 12, no. 3, pp. 1055–1063, 2025.

[21] S. Nápoles, E. Pérez, and F. Smarandache, "Advances in fuzzy cognitive maps: Theory and applications," *Appl. Soft Comput.*, vol. 127, p. 109339, 2022.

[22] M. Elyasi and A. Gharib, "Energy management of plug-in hybrid electric vehicles using fuzzy cognitive maps," *Energy Eng.*, vol. 120, no. 3, pp. 513–527, 2023.

[23] N. Aliyeva *et al.*, "Reducing costs and pollution through solar energy systems using an economic–environmental approach," *Procedia Environ. Sci. Eng. Manag.*, vol. 12, no. 3, pp. 931–939, 2025.

[24] A. Bakhshi and H. Arghavani, "Urban driving cycle modeling for energy optimization," *Energy Rep.*, vol. 8, pp. 6218–6228, 2022.

[25] D. Efimov and A. Gospodarikov, "Technical and technological aspects of using Reuleaux triangular profile rolls in crushing units of ore processing plants," *Min. Inf. Anal. Bull.*, vol. 10–12, pp. 198–204, 2022.

[26] Y. Zhao and J. Zheng, "Driving cycle construction for megacities: A case study," *Sustain. Cities Soc.*, vol. 88, p. 104344, 2023.